Antimonide superlattice barrier infrared detectors

David Z. Ting*, Cory J. Hill, Alexander Soibel, Jean Nguyen, Sam A. Keo, Jason M. Mumolo, Michael C. Lee, Baohua Yang, Sarath D. Gunapala

Jet Propulsion Laboratory, California Institute of Technology,
4800 Oak Grove Drive, Pasadena, California, USA 91109-8099

ABSTRACT

Unipolar barriers can block one carrier type but allow the un-impeded flow of the other. They can be used to implement the barrier infra-red detector (BIRD) design for increasing the collection efficiency of photo-generated carriers, and reducing dark current generation without impeding photocurrent flow. In particular, the InAs/GaSb/AlSb material system, which can be epitaxially grown on GaSb or InAs substrates, is well suited for implementing BIRD structures, as there is considerable flexibility in forming a variety of alloys and superlattices, and tailoring band offsets. We describe our efforts to achieve high-performance long wavelength InAs/GaSb superlattice infrared photodetectors based on the BIRD architecture. Specifically, we report a 10 μm cutoff device based on a complementary barrier infrared detector (CBIRD) design. The detector, without anti-reflection coating, exhibits a responsivity of 1.5 A/W and a dark current density of 1×10^{-5} A/cm^2 at 77K under 0.2 V bias. It reaches 300 K background limited infrared photodetection (BLIP) operation at 101 K, with a black-body BLIP D^* value of 2.6×10^{10} cm-Hz$^{1/2}$/W for 2π field of view under 0.2 V bias.

Keywords: unipolar barrier, heterostructure, infrared, photodetector, superlattice

1. INTRODUCTION

The use of heterostructures to improve HgCdTe infrared detector performance is a well-established practice [1, 2, 3]. Detector structures such as the double-layer heterojunction (DLHJ) have demonstrated significant advantages over their homojunction counter parts. The use of heterostructures is also prevalent in III-V semiconductor based infrared detectors. A particularly useful heterostructure construct is the unipolar barrier. A unipolar barrier is one that can block one carrier type (electron or hole) but allows the un-impeded flow of the other, as illustrated in Fig. 1. The much celebrated concept of the double-heterostructure (DH) laser, which makes use of a pair of complementary unipolar barriers, was first described in 1963 [4, 5], soon after the birth of the idea of heterostructure devices itself. Unipolar barriers are also used to enhance infrared detector performance. A unipolar barrier can be used to impede the flow of majority carrier dark current in photoconductors [6]. A DH detector design, depicted in Fig. 1, can be used to reduce diffusion dark current emanating from the diffusion wings surrounding the absorber layer [7]. The nBn [8, 9] (see Fig. 1) or XBn [10] detector structure uses a unipolar barrier to suppress dark current associated with Shockley-Read-Hall processes without impeding photocurrent flow, and to suppress surface leakage current [9]. In general, unipolar barriers can be used to implement the barrier infra-red detector (BIRD) architecture for increasing the collection efficiency of photo-generated carriers, and reducing dark current generation without inhibiting photocurrent flow.

* David.Z.Ting@jpl.nasa.gov; Ph: +1.818.354.1549; FAX: +1.818.393.4663

Infrared Systems and Photoelectronic Technology IV,
edited by Eustace L. Dereniak, John P. Hartke, Paul D. LeVan, Randolph E. Longshore, Ashok K. Sood,
Proc. of SPIE Vol. 7419, 74190B · © 2009 SPIE · CCC code: 0277-786X/09/$18 · doi: 10.1117/12.829047

Downloaded from SPIE Digital Library on 29 Nov 2009 to 159.226.100.225. Terms of Use: http://spiedl.org/terms

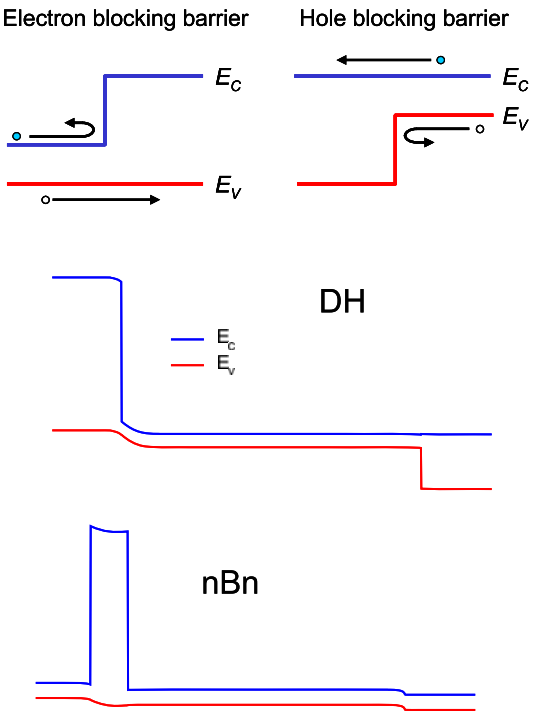

Fig. 1 Schematic illustrations of electron- and hole-blocking unipolar barriers, and two examples of unipolar barrier based device structures: double heterostructure (DH), and nBn structure.

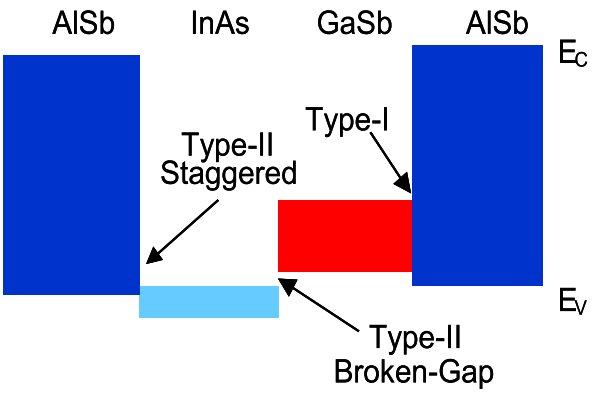

Fig. 2 Schematic illustration of the energy band alignment in the nearly lattice matched InAs/GaSb/AlSb material system. The solid colored rectangles indicate the relative positions of the InAs, GaSb and AlSb energy band gaps. Three types of band alignment are available in this material system: (1) type-I (nested) band alignment between GaSb and AlSb, (2) type-II staggered alignment between InAs and AlSb, and (3) type-II broken gap (or type-III) alignment between InAs and GaSb.

For bulk infrared semiconductor absorber material, unipolar barriers are not always readily attainable, as both the absorber and barrier materials require (near) lattice matching to available substrates, and the proper band offsets must exist between the absorber and the barrier. Considerable effort and ingenuity may be required find work-arounds if an ideal match cannot be found [7]. The task of building unipolar barriers can be made easier with artificially engineered materials such as superlattices. The nearly lattice-matched InAs, GaSb, AlSb material system, which can be epitaxially grown on GaSb or InAs substrates, is well suited for building absorber/unipolar barrier pairs, and for implementing BIRD structures. As illustrated in Fig. 2, with the availability of type-I nested, type-II staggered (straddling), and type-II broken-gap (misaligned, or type III) band offsets between the GaSb/AlSb, InAs/AlSb, and InAs/GaSb material pairs, respectively, there is considerable flexibility in forming a rich variety of alloys and superlattices. The type-II broken-gap InAs/Ga(In)Sb superlattice can be used as mid- or long-wavelength infrared absorber. Superlattices or alloys build from the InAs/GaSb/AlSb material system (often referred to as the antimonide material system, or the antimonides) can also be tailor-designed to build matching unipolar barriers to the infrared absorber superlattices. In particular, the ability to tune the positions of the conduction and valence band edges independently in a type-II superlattice is especially helpful in the design of unipolar barriers. Examples of the broken-gap superlattice based BIRDs are the superlattice nBn [11], the superlattice DH [12,13], the graded-gap W-superlattice based DH structure [14], and the superlattice CBIRD structure [15].

In building BIRD structures with antimonide superlattices, it is helpful to recognize the properties of superlattices that set them apart from bulk semiconductors. In Sec. 2, we discuss the properties of antimonide superlattices. In Sec. 3 we present our recent results on a high-performance antimonide superlattice long-wavelength infrared (LWIR) detector based on the BIRD design. A summary is given in Sec. 4.

Downloaded from SPIE Digital Library on 29 Nov 2009 to 159.226.100.225. Terms of Use: http://spiedl.org/terms

2. ANTIMONIDE SUPERLATTICES

In this section, we examine the properties of the antimonide superlattice infrared detector through a historical perspective. We then explore some theoretical aspects of the antimonide superlattices as related to device properties.

2.1 Historical perspective

In 1977, Sai-Halasz, Tsu, and Esaki [16] proposed a new type of bilayer semiconductor superlattice in which the lower conduction band (CB) edge is located in one material, while the higher valence band (VB) edge is in the other. In this kind of superlattice, the wave functions of the lowest conduction subband and the highest valence subband are localized in the two different host semiconductors (spatially delocalized), and therefore the positions of the CB edge and the VB edge can be, to first order, tuned independently (see Fig. 3). It was suggested that this type of superlattice could be realized using InGaAs/GaSbAs. It was also pointed out in particular that the CB edge of InAs was expected to be lower than the VB edge of GaSb (in what is now called the broken-gap band alignment), and this would lead to interesting behavior since the superlattice CB and VB states are close in energy and could therefore interact. This new type of superlattice, in which the band gaps of the two host semiconductor are either in a staggered or in a broken-gap alignment, was called "type II", to distinguish it from the "type I" superlattice original proposed by Esaki and Tsu [17], in which the band gaps are in a nested alignment. In the literature, "type-II broken-gap" is sometimes referred to as "type-III", to distinguish it from "type-II staggered" [18, 19, 20]. Note however that "type-III" is also used by some authors in the infrared detector literature to refer to superlattices consisting of alternating layers of an inverted band structure zero-gap semiconductor and a normal wider gap semiconductor (e.g., the HgTe/CdTe superlattice) [21]. H. Kroemer advocates using only the descriptive names of nested (or straddling), staggered, and broken-gap (or misaligned), and doing away with numerical designation of types I, II, and III altogether. In any case, in 1978, Sai-Halasz and co-workers demonstrated infrared absorption in an InAs/GaSb superlattice with a ~0.35 eV band gap [22].

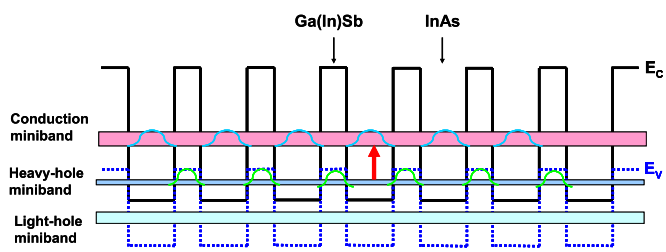

Fig. 3 Schematic energy band diagram of an InAs/Ga(In)Sb broken-gap superlattice illustrating the spatial separation of the conduction band and the heavy-hole band wave functions. The arrow indicates the infrared transition.

The concept of the antimonide superlattice as an infrared detector material was heavily influenced by development in HgCdTe (MCT) infrared detectors. In 1979, Schulman and McGill proposed the use of the CdTe/HgTe superlattice as an infrared material, with possible uniformity advantages over the MCT alloy [23]. Their paper mentioned the use of the InAs/GaSb superlattice as an alternative infrared material, but expressed concerns for the small optical matrix element due to the fact that electron and hole wave functions of the states involved in the infrared transition are spatially separated in a type-II superlattice (see Fig. 3). Later, in 1983, Smith, McGill, and Schulman revisited the theory of CdTe/HgTe superlattices, and pointed out some key advantages of superlattices over bulk materials for infrared detection: (1) superlattices have weaker cutoff wavelength dependence on composition than the MCT alloy, and are therefore less susceptible to variations due to composition fluctuation, (2) superlattices have reduced p-side diffusion current due to the larger electron mass, and, (3) superlattice tunneling lengths are shorter than for MCT alloys with the same band gap, and therefore have reduced band-to-band tunneling [24]. These properties apply to the InAs/GaSb superlattice as well. To address the issue of small oscillator strength in InAs/GaSb superlattices, in 1987 Smith and Mailhiot proposed the type II InAs/GaInSb strained layer superlattice (SLS) infrared detector [25]. The SLS has larger optical matrix elements than the InAs/GaSb superlattice. Although the optical matrix element of the type-II SLS is still smaller than that in bulk MCT, its absorption coefficient is comparable to that of MCT because of the higher joint density of states. The electron effective mass for a 10 μm cutoff SLS is ~0.04 m_0 (0.0088 m_0 for MCT of comparable cutoff wavelength), which is large enough to reduce band-to-band tunneling, and still small enough to provide good

Downloaded from SPIE Digital Library on 29 Nov 2009 to 159.226.100.225. Terms of Use: http://spiedl.org/terms

electron mobility. In 1990, Miles, Chow, Schulman and McGill experimentally demonstrated LWIR absorption in InAs/GaInSb strained layer superlattices [26].

D. L. Smith also postulated that Auger recombination rates in superlattices should be lower than those in bulk semiconductors due to the splitting of the heavy hole (hh) and light hole (lh) bands, and the larger electron effective mass. Smith communicated the idea to McGill [27], who in turn stimulated H. Ehrenreich's group to perform detailed calculations to put this concept on a firm theoretical basis. In 1992, Grein, Young, and Ehrenreich presented a theoretical analysis which showed that p-type Auger lifetimes in a 11 μm cutoff InAs/InGaSb SLS at 77K could be 3-5 orders of magnitude longer than those of bulk MCT with the same gap [28]. Experimental measurements of Auger lifetime enhancement in InAs/GaInSb superlattices were reported in 1994 [29]. As the material quality of antimonide superlattices improves, and defect related dark currents decrease, the long Auger lifetimes could yield real advantages in LWIR antimonide superlattice detectors. Some of the other fundamental studies that are important for the development of this technology includes the theoretical calculation of InAs/GaSb optical properties using a realistic band structure model [30], the influence of interface types [31], and cross-sectional scanning electron microscopy studies of antimonide superlattices [32,33]. In 1996, researchers at UCSB demonstrated an InAs/GaInSb SLS LWIR photodiode based on a double heterojunction design [12].

The demonstration of high-performance InAs/GaInSb infrared photodiodes by Fuchs and co-workers at Fraunhofer IAF in 1997 [34] generated strong interest in the antimonide superlattices. Since then, the area has seen rapid progress, with photodetector and FPA results reported by many groups [15,35,36,37,38,39,40]. It is interesting to note that while the oscillator strength of the InAs/GaSb superlattice is not as strong as that of the InAs/GaInSb SLS, both types of antimonide superlattices are being actively investigated today. In particular, Prof. Razeghi's group at Northwestern has been reporting results on the InAs/GaSb superlattice since 1998 [41]. While the oscillator strength of the InAs/GaSb SL is weaker, like its InAs/GaInSb SLS counterpart it also has a higher joint density of states than bulk semiconductors, and therefore has an adequately large absorption coefficient. The InAs/GaSb superlattice, which uses unstrained and minimally strained binary semiconductor layers, may also have material quality advantages over the SLS, which uses a strained ternary semiconductor (GaInSb). Most recently, the use of superlattice heterostructures as well as superlattices with complex supercells, such as the "W" [37] and the "M" [35] superlattices, has resulted in very substantial performance gains over homojunction devices. In the future, we expect high-performance LWIR superlattice detectors to be primarily of heterostructure designs.

We note that the term SLS is sometimes used in the literature to refer to both the InAs/GaSb and the InAs/GaInSb superlattices. It is true that the slight lattice mismatch (0.6%) between InAs and GaSb can cause sufficient strain build up to affect material quality in very thick InAs/GaSb superlattices. However, this is an easily resolvable issue for InAs/GaSb superlattices grown on GaSb substrates, for which InSb-like interfaces can be used to provide strain balance. In this work, we reserve the term SLS for InAs/GaInSb superlattices, where the GaInSb layers are intentionally strained for the purpose of increasing oscillator strength [25]. Note that interface engineering techniques can also be applied to minimize the average strain in the InAs/GaInSb SLS, as has been demonstrated by the work from the Fraunhofer IAF [34].

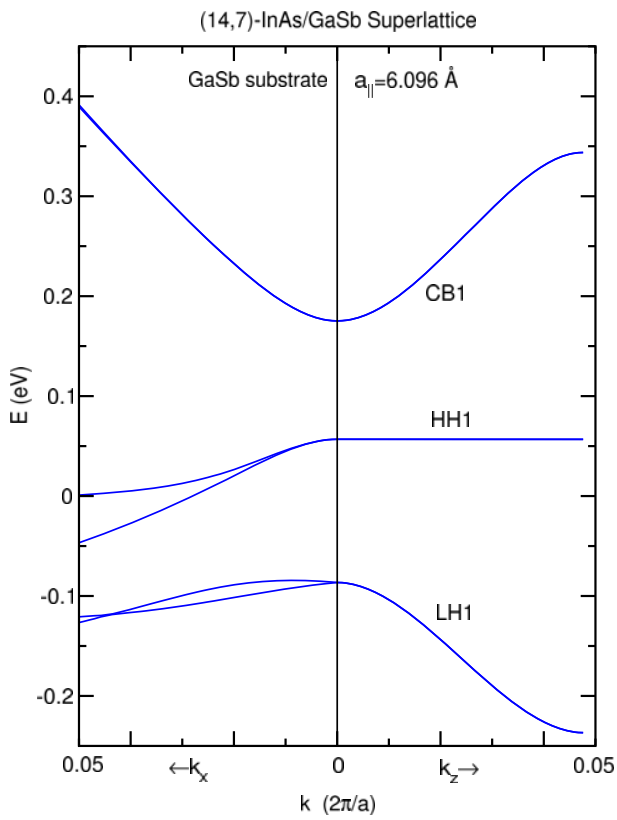

Fig. 4 Conduction and valence band structure emanating from the zone center along an in-plane direction (k_x) and the growth direction (k_z), with k_y = 0, for a long wavelength infrared superlattice. Each superlattice period consists of L_z=21 monolayers (MLs), with 14 MLs of InAs and 7 MLs of GaSb.

Downloaded from SPIE Digital Library on 29 Nov 2009 to 159.226.100.225. Terms of Use: http://spiedl.org/terms

2.2 Theoretical aspects

In constructing superlattice based infrared detector structures, special considerations should be given to the absorber superlattice intrinsic properties, many of which are revealed by band structure. Fig. 4 shows the band structure of a typical LWIR broken-gap superlattice, calculated using an enhanced effective bond orbital model [42]. The main features of the superlattice band structure that distinguishes it from that of the typical bulk semiconductor are that (1) the splitting of the highest heavy hole band (HH1) and the highest light hole band (LH1) at the zone center, and, (2) the HH1 band is nearly dispersionless along the growth direction. While the infrared absorption edge is determined by the gap between the lowest conduction band (CB1) and the HH1 band, the electron effective mass is determined by the CB1-LH1 gap. In unstrained bulk semiconductors, the two gaps are the same. In the superlattice, the larger CB1-LH1 gap leads to a large electron effective mass, which is beneficial for reducing band-to-band tunneling. Both the dispersionless HH1 band structure and the increased electron effective mass contribute to a larger joint density of states (JDOS). This results in a larger absorption coefficient, which, to first order, is directly proportional to the JDOS. This helps to compensate for the small optimal matrix element disadvantage inherent in type II superlattices. As mentioned previously, the splitting of the HH1 and LH1 bands can also help in reducing Auger recombination.

The band structure in Fig. 4 reveals important information about carrier transport properties which can affect detector design. We note that the CB1 band shows strong dispersion along both the growth (z) and an in-plane direction (x), while the HH1 band is highly anisotropic and appears nearly dispersionless along the growth (transport) direction. We expect the electron and hole density of states to be 3D- and 2D-like, respectively. The calculated conduction and valence subband zone center effective masses along the x and z directions are: $m_c^x* = 0.021m_0$ and $m_c^z* = 0.021m_0$, and $m_{hh1}^x* = 0.031m_0$ and $m_{hh1}^z* = 38m_0$. Recalling that carrier group velocity is given by $\mathbf{v} = \nabla_{\mathbf{k}} E(\mathbf{k}) / \hbar$, where $E(\mathbf{k})$ describes the band structure, we would expect very low hole mobility and diffusivity along the growth direction. Therefore, for this LWIR superlattice absorber, detector designs based on hole transport would be rather unfavorable. Moreover, in general low mobility of holes can also slow down the electrons, since excess electrons and holes are coupled through coulomb interaction in ambipolar transport. We should point out that the hole mobility for MWIR superlattices are not nearly as low. The calculated conduction and valence subband zone center effective masses for the

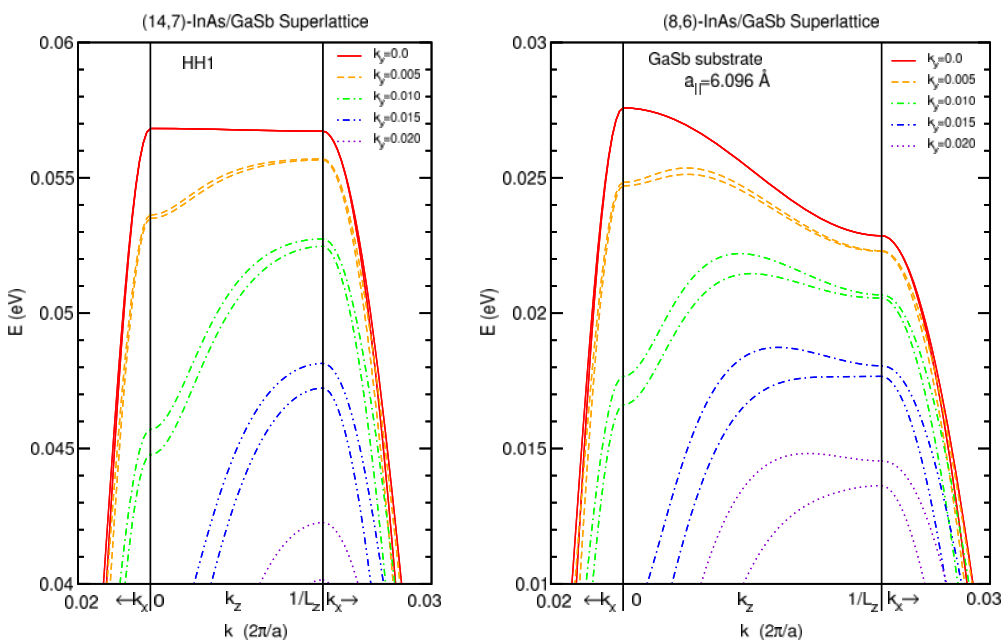

Fig. 5 (14,7)-InAs/GaSb superlattice (left) and (8,6)-InAs/GaSb superlattice (right) HH1 subband band structure. In each graph, the central panel shows band structure along the growth direction (k_z) from the reduce zone center to the zone boundary. The side panels show the continuation of the band structure plotted along the in-plane direction k_x. The HH1 bands for several k_y values are plotted. In each graph, L_z is the number of monolayers in each period of the superlattice (21 and 14, respectively, for the graphs on the left and right side). For reference, the value of $2k_BT$ is ~14 meV at T=80K.

Downloaded from SPIE Digital Library on 29 Nov 2009 to 159.226.100.225. Terms of Use: http://spiedl.org/terms

(8,6)-InAs/GaSb MWIR superlattice along the x and z directions are: $m_c^x* = 0.025m_0$ and $m_c^z* = 0.024m_0$, and $m_{hh1}^x* = 0.037m_0$ and $m_{hh1}^z* = 1.85m_0$. Note that this MWIR superlattice HH1 effective mass is ~20 times smaller than for the LWIR superlattice.

Even for the LWIR superlattice, a closer look at the HH1 band structure reveals that the hole velocity may not be as low as first appeared. The graph on the left side of Fig. 5 shows that in the LWIR superlattice, for $k_y = 0$, the HH1 band has very little dispersion along k_z (z being the growth direction), with maximum occurring at the center of the reduced Brillouin zone. But as the result of interaction with other subbands, the HH1 band dispersion along the growth direction becomes appreciably larger as the in-plane momentum (k_y) increases; the band maximum along the k_z direction quickly switches from the reduced zone center to the zone boundary. At lower temperatures, we expect holes to occupy the less dispersion portions of the HH1 band, for which the hole density of states (DOS) is more 2D-like, and hole velocities along the growth direction are low. At higher temperatures, we expect the more dispersive parts of the HH1 to be occupied also. The thermalized holes would occupy the part of the DOS that is more 3D-like, and would attain higher velocities. The right side of Fig. 5 shows the corresponding HH1 band structure plot for the (8,6)-InAs/GaSb MWIR superlattice. Note that in this case, the HH1 band shows a reasonable amount of dispersion even at $k_y = 0$, and its hole transport properties should be much better than that of the LWIR superlattice. Fig. 6 shows the actual calculated density of states for the (14,7)-InAs/GaSb LWIR superlattice and the(8,6)-InAs/GaSb MWIR superlattice. The conduction band DOS resembles the standard 3D DOS ($\propto \sqrt{E - E_c}$), although with some modifications due to band non-parabolicity. The HH1 DOS differs qualitatively from both the standard 3D and the 2D (step-like) DOS. The form of the DOS can affect our understanding of device performance. A standard tool used to study detector characteristics is dark current analysis, in which we fit experimentally measured dark current to analytical forms for various dark current sources (diffusion, generation-recombination, tunneling). This allows us to extract information on the dark current generating mechanisms and carrier lifetimes [43]. In the typical dark current analysis, the carrier densities are modeled using the standard 3D DOS appropriate for bulk semiconductors. But as shown in Fig. 6, superlattice DOS (especially VB DOS) can be quite different from bulk DOS. This can affect the accuracy of dark current analysis. We note that there is tentative indirect evidence from LWIR superlattice infrared detector dark current analysis that the hole density switches from 2D- to 3D-like with increasing temperature [44].

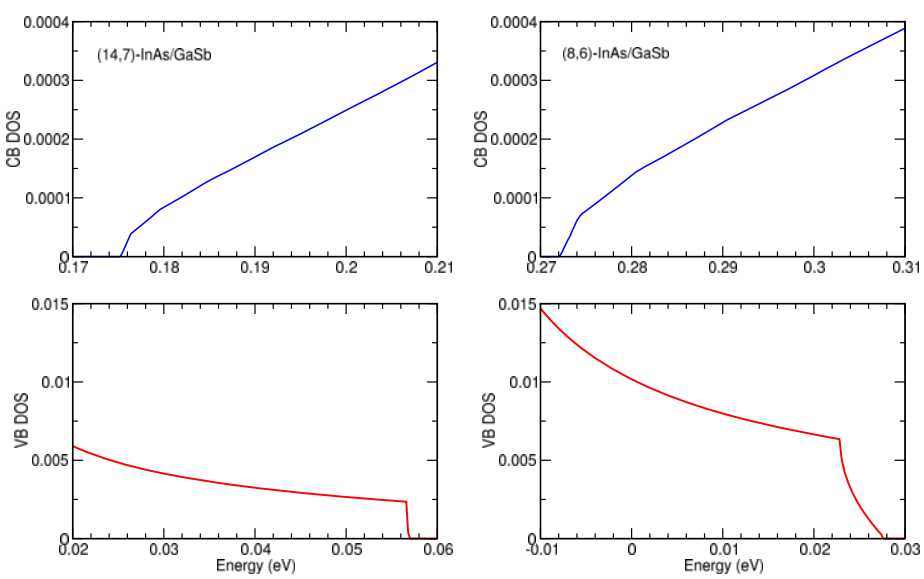

Fig. 6 Conduction and valence band edge density of states (DOS) for the (14,7)-InAs/GaSb superlattice (left) and the (8,6)-InAs/GaSb superlattice (right). The valence band DOS shown originates from the HH1 subband.

Downloaded from SPIE Digital Library on 29 Nov 2009 to 159.226.100.225. Terms of Use: http://spiedl.org/terms

3. SUPERLATTICE HETEROSTRUCTURE BARRIER INFRARED DETECTORS

In this section, we discuss the construction of unipolar barriers for antimonide superlattices, and then present results on a superlattice barrier infrared detector built using the unipolar barriers.

3.1 Unipolar barriers for antimonide superlattices

As discussed in Sec. 1, the InAs/GaSb/AlSb material system is highly flexible. It enables the formation of a rich variety of alloys and superlattices, and is well suited for building absorber/unipolar barrier pairs for implementing BIRD structures. In this sub-section we illustrate the design of unipolar barriers for an antimonide superlattice. We use the (14,7)-InAs/GaSb superlattice LWIR absorber in our example. To construct an electron-blocking unipolar barrier, we use the (7,7)-InAs/GaSb electron-barrier (eB) SL. Recall that the valence band states in the InAs/GaSb superlattices are localized in the GaSb layers (see Fig. 2). Keep the GaSb layer thickness the same in the absorber SL and the eB SL ensures the approximate valence band edge alignment. The narrower InAs layer width in the eB SL pushes its conduction band edge higher than that of the absorber SL, allowing it to act as an electron barrier to electrons from the absorber SL. Fig. 7 shows the band structure of the absorber SL and the eB SL. The valence subband edges of the absorber SL and eB SL are in approximate alignment, but the conduction subband edges shows an offset of approximately 150 meV.

Similarly, we can also construct a hole-blocking unipolar barrier for the (14,7)-InAs/GaSb absorber SL. We use a (15,4)-InAs/AlSb superlattice as the hole-barrier (hB) SL. Fig. 7 shows the absorber SL and hB SL have nearly matched conduction subband edges, but have a relatively large valence subband offset of 340 meV. We noted that many design variations of unipolar barriers are possible with the InAs/GaSb/AlSb material system. For instance, the 4-layer InAs/GaSb/AlSb/GaSb M-structure hB SL [45] has already demonstrated its effectiveness in LWIR focal plane array (FPA) applications [35].

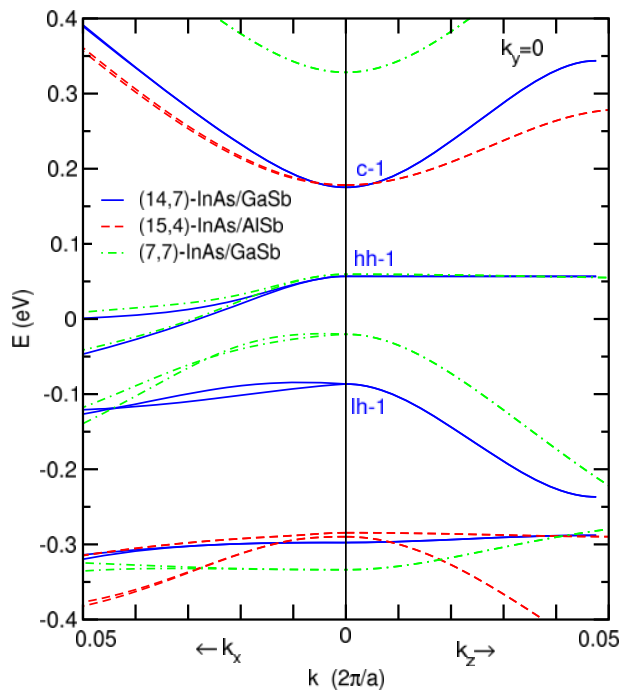

Fig. 7 Conduction and valence band structure emanating from the zone center along an in-plane direction (k_x) and the growth direction (k_z), with $k_y = 0$, for three superlattices. Each period of the absorber superlattice, labeled by (14,7)-InAs/GaSb, consists of 14 monolayers (MLs) of InAs and 7 MLs of GaSb. The conduction band, heavy-hole 1 and light-hole 1 band edges of the absorber SL are respectively labeled c-1, hh-1, and lh-1 in the figure. Also shown are the band structures for a matching (15,4)-InAs/AlSb hole-barrier SL, and a (7,7)-InAs/GaSb electron-barrier SL.

3.2 Antimonide superlattice barrier infrared detector

In this sub-section we present our recent results on a high-performance antimonide superlattice LWIR detector. The detector is based on a complementary barrier infrared detector (CBIRD) design, consisting of an InAs/GaSb absorber SL sandwiched between an InAs/AlSb hole-barrier (hB) SL, and an InAs/GaSb electron-barrier (eB) SL, similar to the designs described above. As discussed earlier, we expect the InAs/GaSb LWIR SL to have more favorable electron transport properties, therefore the absorber superlattice is doped lightly p-type, so that we have better minority carrier (electron) mobility. A full description of the device structure is published elsewhere [15]. Figure 8 shows calculated energy band diagrams of the CBIRD device. The top panel shows the unbiased band diagram. The bottom panel shows the band diagram of the device under a small reverse bias.

Downloaded from SPIE Digital Library on 29 Nov 2009 to 159.226.100.225. Terms of Use: http://spiedl.org/terms

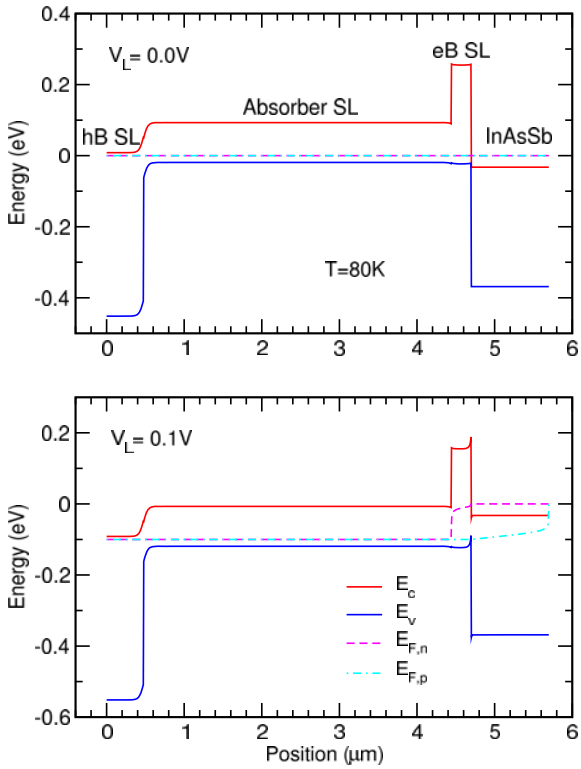

Fig. 8 Calculated energy band diagram of a complementary barrier infrared detector structure showing conduction band edge, valence band edge, and electron and hole quasi-Fermi levels under 0 V (top panel) and 0.1 V (bottom panel) applied bias.

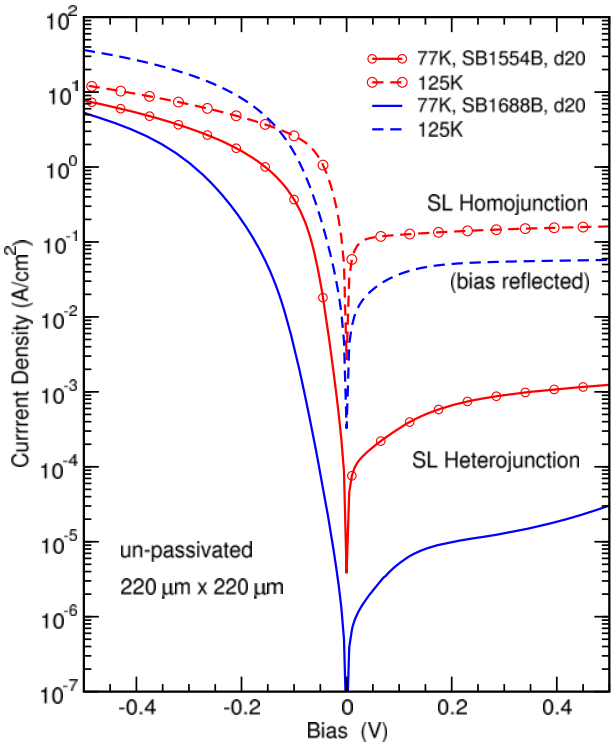

Fig. 9 Dark current densities for a superlattice homojunction LWIR detector and a superlattice heterojunction LWIR detector taken at 77K and 125K. The heterojunction device is reverse-biased under positive applied bias. The homojunction device J-V curves are reflected about the y-axis for easy comparison. The devices are not passivated.

The device structure was grown on a 50-mm diameter Te-doped GaSb (100) substrate in a Veeco Applied-Epi Gen III molecular beam epitaxy chamber equipped with valved cracking sources for the group V Sb2 and As2 fluxes. Standard contact mode optical lithography was used to define the patterns for square mesas of area 220×220 μm^2. After pattern development, the wafer was etched in a citric acid based wet chemical etching solution to isolate individual devices. Following another lithography step to define the opening for contact metals, Ti/Pt/Au was deposited for both top and bottom ohmic contacts. There was no passivation, anti-reflection coating, or metal annealing. The photodiodes were mounted in a ceramic package using indium, and wire-bonded before testing for dark current and responsivity. The photocurrent response to a grating-based monochrometer source was normalized by that of a pyroelectric detector to arrive at the relative spectral responsivity. The absolute spectral responsivity is obtained by scaling the relative spectral responsivity according to the total photocurrent response to a 1000 K blackbody radiation source in a known spectral window. Dark current measurements were made by immersing the sample in a Dewar containing liquid helium or liquid nitrogen. In each measurement setup the device packages were placed in contact with a computer-controlled resistive heater in order to measure device characteristics at various temperatures.

Figure 9 shows the measured dark current densities for two detectors with the same LWIR superlattice absorbers, one based on a homojunction design, and another based on the CBIRD design. The two detectors have approximately the same photo-response. However the CBIRD shows a substantial dark current reduction over the homojunction superlattice detector. Note that the CBIRD under consideration is an electron collecting device, therefore it is reverse-biased under a positive applied bias. The homojunction diode is hole-collecting device; we reflected its J-V curves about the vertical axis for easy comparison to the CBIRD.

Downloaded from SPIE Digital Library on 29 Nov 2009 to 159.226.100.225. Terms of Use: http://spiedl.org/terms

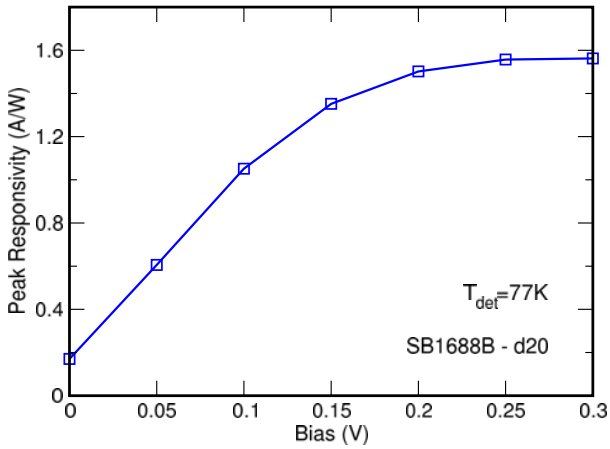

Fig. 10 The single-pass peak responsivity as a function of applied bias for a top illuminated CBIRD device without anti-reflection coating, measured at 77 K.

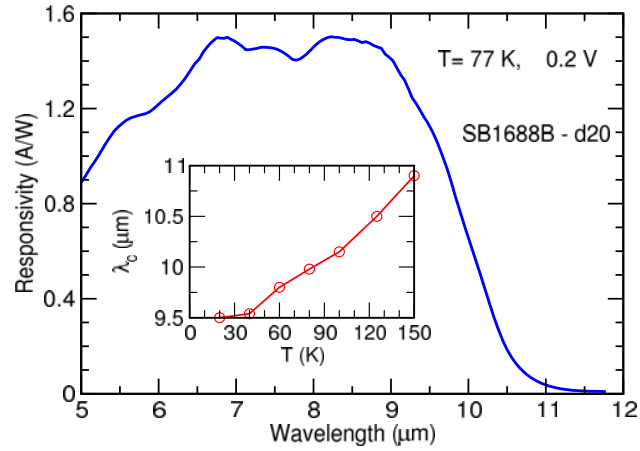

Fig. 11 Top illuminated single-pass spectral responsivity for a CBIRD device without anti-reflection coating under 0.2 V applied bias, measured at 77 K. The inset shows the detector cutoff wavelength as a function of temperature.

We fabricated a large-area (220×220 μm^2 in size), device for responsivity measurements. The devices is unpassivated, and does not have anti-reflection coating. Figure 10 shows the peak responsivity of the CBIRD device as a function of applied bias, taken at 77 K. We observe that the photoresponse increases with bias from 0 to ~0.2 V, and then plateaus for bias greater than 0.2 V. This property is beneficial for the uniform response in FPAs, where we could operate in the plateau region and tolerate small detector-to-detector applied bias variations in the array. Note that even though the device is best operated under a small bias, as can be seen in Fig. 9, the 77 K dark current density at 0.2 V is still quite low, with a value of ~1×10^{-5} A/cm^2. Figure 11 shows the spectral response of measured under 0.2 V applied bias at 77 K. The device has a 10 μm cutoff (defined by 50% peak responsivity), with a peak responsivity of 1.5 A/W. The inset of Fig. 11 shows that that the cutoff wavelength decreases with the lowering of the temperature, changing from 10.9 μm at 150 K to 9.4 μm at 20 K. The device has a zero-bias dynamic resistance-area product of R_0A =14,000 ohm-cm^2 at 77 K, which is the highest value for a 10 μm cutoff SL detectors reported to date. However we need to point out that while R_0A is useful for characterizing Johnson noise limited photovoltaic detectors operating near zero bias, it is less relevant for this detector, which operates at a higher bias (~0.2 V) where shot noise dominates. Here it is more appropriate to examine the dark current density under the operating bias for determining detector noise spectrum.

We also calculated the shot-noise limited black-body D^*, where the noise spectrum is determined by the measure dark current and photocurrent integrated over the 8 μm to 10 μm spectral range (the overlap between the atmospheric window and the detector cutoff). Figure 12 shows the 300 K background black-body D^* as a function of applied bias for f/2 optics and for 2π field of view, with the detector operating at 77 K. We take the background limited infrared photodetection (BLIP) condition to be where the dark current is ¼ of the photocurrent. As reported elsewhere [15], under 0.2 V, the detector reaches 300 K BLIP operation at 86 K with a black-body BLIP D^* value of 1.1×10^{11} cm-Hz$^{1/2}$/W for f/2 optics. For 300K background with 2π field of view, the device shows a BLIP temperature of 101 K with a black-body BLIP D^* value of 2.6×10^{10} cm-Hz$^{1/2}$/W.

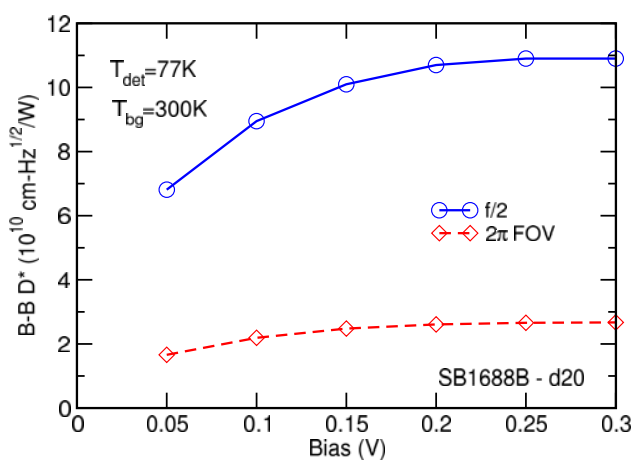

Fig. 12 The 300 K background black-body D^* as a function of applied bias for f/2 optics and for 2π field of view, with the detector operating at 77 K.

Downloaded from SPIE Digital Library on 29 Nov 2009 to 159.226.100.225. Terms of Use: http://spiedl.org/terms

4. SUMMARY

We discuss the general concept of unipolar barriers and how they can be used to improve infrared detector performance. We identify the antimonide superlattice as a good candidate for building unipolar barrier based barrier infrared detectors (BIRDs) due to the flexibility of the InAs/GaSb/AlSb material systems. We examined the basic properties of the antimonide superlattice infrared detector through a historical perspective. We also explored some theoretical aspects of the antimonide superlattices as related to device properties, pointing out in particular that the band structure of LWIR InAs/GaSb favors electron transport. We report device results on an InAs/GaSb superlattice based complementary barrier infrared detector (CBIRD), which demonstrates significant performance advantages over homojunction superlattices in infrared detection.

Acknowledgment

The authors thank X. Cartoixà, J. N. Schulman, and E. R. Blazejewski for helpful discussions, and M. Tidrow, R. Liang and P. Dimotakis for encouragement and support. The research described in this publication was sponsored by the Missile Defense Agency, and was carried out at the Jet Propulsion Laboratory, California Institute of Technology, under a contract with the National Aeronautics and Space Administration.

REFERENCES

1. J. M. Arias, J. G. Pasko, M. Zandian, S. H. Shin, G. M. Williams, L. O. Bubulac, R. E. De Wames, and W. E. Tennant, "Planar p-on-n HgCdTe heterostructure photovoltaic detectors, " *Appl. Phys. Lett*. **62**, 976 (1991).
2. G. N. Pultz, P. W. Norton, E. E. Kruger, and M. Reine, "Growth and characterization of P-on-n HgCdTe liquid-phase epitaxy heterojunction material for 11–18 μm applications," *J. Vac. Sci. Technol. B* **9**, 1724 (1991).
3. T. Tung, L. V. DeArmond, R. F. Herald, P. E. Herning, M. H. Kalisher, D.A. Olson, R. F. Risser, A. P. Stevens, and S. J. Tighe, "State of the art of Hg-melt LPE HgCdTe at Santa Barbara Research Center," Proc. SPIE 1735,109 (1992).
4. H. Kroemer, "A proposed class of heterojunction injection lasers," *Proc. IEEE* **51**(12), 1782 (1963).
5. Zh. I. Alferov, R. F. Kazarinov, Inventor's Certificate No. 181737 (in Russian), Application No. 950 840 (1963).
6. A. M. White, "Infra red detectors," U. S. Patent No. 4,679,063 (7 July 1987).
7. M. Carras, J. L. Reverchon, G. Marre, C. Renard, B. Vinter, X. Marcadet, and V. Berger, "Interface band gap engineering in InAsSb photodiodes," *Appl. Phys. Lett*. **87**(10) 102103 (2005)
8. S. Maimon and G. W. Wicks, "nBn detector, an infrared detector with reduced dark current and higher operating temperature," *Appl. Phys. Lett*. **89**(15) 151109 (2006).
9. J. R. Pedrazzani, S. Maimon and G. W. Wicks, "Use of nBn structures to suppress surface leakage currents in unpassivated InAs infrared photodetectors," *Electronics Lett*. **44**(25) 1487-1488 (2008).
10. P. Klipstein, "'XBn' barrier photodetectors for high sensitivity and high operating temperature infrared sensors," *Proc. of SPIE*. 6940 (2009) 69402U.

Downloaded from SPIE Digital Library on 29 Nov 2009 to 159.226.100.225. Terms of Use: http://spiedl.org/terms

11. J. B. Rodriguez, E. Plis, G. Bishop, Y. D. Sharma, H. Kim, L. R. Dawson, and S. Krishna, "nBn detectors based on InAs/GaSb type-II strain layer superlattice," *Appl. Phys. Lett*. **91**(4) 043514 (2007).

12. J. L. Johnson, L. A. Samoska, and A. C. Gossard, J. L. Merz, M. D. Jack, G. R. Chapman, B. A. Baumgratz, K. Kosai, and S. M. Johnson, "Electrical and optical properties of infrared photodiodes using the InAs/$Ga_{1-x}In_xSb$ superlattice in heterojunctions with GaSb," *J. Appl. Phys. Lett*. **80**(2) 1116-1127 (1996).

13. B.-M. Nguyen, D. Hoffman, E. K.-W. Huang, P.-Y. Delaunay, and M. Razeghi, "Background limited long wavelength infrared type-II InAs/GaSb superlattice photodiodes operating at 110 K," *Appl. Phys. Lett*. **93**(12) 123502 (2008).

14. I. Vurgaftman, E. H. Aifer, C. L. Canedy, J. G. Tischler, J. R. Meyer, J. H. Warner, E. M. Jackson, G. Hildebrandt and G. J. Sullivan, "Graded band gap for dark-current suppression in long-wave infrared W-structured type-II superlattice photodiodes," *Appl. Phys. Lett*. **89**(12), 121114 (2006).

15. D. Z.-Y. Ting, C. J. Hill, A. Soibel, S. A. Keo, J. M. Mumolo, J. Nguyen, and S. D. Gunapala, "A high-performance long wavelength superlattice complementary barrier infrared detector," *Appl. Phys. Lett*. **95**, 023508 (2009).

16. G. A. Sai-Halasz, R. Tsu, and L. Esaki, "A new semiconductor superlattice," *Appl. Phys. Lett*. **30**(12), 651-653 (1977).

17. L. Esaki and R. Tsu, "Superlattice and negative differential conductivity," *IBM J. Res. Dev*. **14**, 61-65 (1970).

18. J. H. Davies, [*The Physics of Low Dimensional Semiconductors: An Introduction*], Cambridge University Press, Cambridge, New York, and Melbourne, 86-87 (1998).

19. D. Dragoman and M. Dragoman, [*Optical Characterization of Solids*], Springer-Verlag, Berlin, Heidelberg and New York, 258-259 (2002).

20. S. M. Sze and K. K. Ng, [*Physics of Semiconductor Devices*, 3rd Edition], Wiley, New Jersey, 58 (2007).

21. Michael A. Kinch, [*Fundamentals of Infrared Detector Materials*], SPIE Press, Bellingham, 45 (2007).

22. G. A. Sai-Halasz, L. L. Chang, J.-M. Welter, C.-A. Chang and L. Esaki, "Optical absorption of $In_{1-x}Ga_xAs$-$GaSb_{1-y}As_y$ superlattices," *Solid State Commun. Phys*. **27**, 935-937 (1978).

23. J. N. Schulman and T. C. McGill, "The CdTe/Hg/Te superlattice: Proposal for a new infrared material," *Appl. Phys. Lett*. **34**(10), 663 (1979).

24. D. L. Smith, T. C. McGill, and J. N. Schulman, "Advantages of the HgTe-CdTe superlattice as an infrared detector material," *Appl. Phys. Lett*. **43**(2), 180 (1983).

25. D. L. Smith and C. Mailhiot, "Proposal for strained type II superlattice infrared detectors," *J. Appl. Phys.* **62**(6), 2545 (1987).

26. R. H. Miles, D. H. Chow, J. N. Schulman, and T. C. McGill, "Infrared characterization of InAs/$Ga_{1-x}In_xSb$ superlattices," *Appl. Phys. Lett*. **57**(8), 801 (1990).

27. D. H. Chow R. H. Miles, D. A. Collins, J. N. Schulman, and T. C. McGill, "Type-II superlattices for infrared detectors and devices," *Semicond. Sci. Technol.* **6**, C47-C51 (1991).

28. C. H. Grein, P. M. Young, and H. Ehrenreich, "Minority carrier lifetimes in ideal InGaSb/InAs superlattices," *Appl. Phys. Lett*. **61**(24), 2905 (1992).

29. E. R. Youngsdale, J. R. Meyer, C. A. Hoffman, F. J. Bartoli, C. H. Grein, P. M. Young, H. Ehrenreich, R. H. Miles, and D. H. Chow, "Auger lifetime enhancement in InAs-$Ga_{1-x}In_xSb$ superlattices," *Appl. Phys. Lett*. **64**(23), 3160 (1994).

30. Y.-C. Chang and J. N. Schulman, "Interband optical transitions in GaAs-$Ga_{1-x}Al_xAs$ and InAs-GaSb superlattices," *Phys. Rev. B* **31**(4), 2069 (1985).

Downloaded from SPIE Digital Library on 29 Nov 2009 to 159.226.100.225. Terms of Use: http://spiedl.org/terms

31. R. H. Miles, J. N. Schulman, D. H. Chow and T. C. McGill, "Electronic band structure of far-infrared $Ga_{1-x}In_xSb$/InAs superlattices," *Semicond Sc. Technol. Phys.* **8**, S102-S105 (1993).

32. A. Y. Lew, S. L. Zuo, E. T. Yu, and R. H. Miles, "Correlation between atomic scale structure and mobility anisotropy in InAs/$Ga_{1-x}In_xSb$ superlattices," *Phys. Rev. B* **57**(11), 6534 (1998).

33. J. Steinshnider, J. Harper, M. Weimer, C.-H. Lin, S.-S. Pei, and D. H. Chow, "Origin of antimony segregatin in GaInSb/InAs strained-layer superlattices," *Phys. Rev. Lett.* **85**(21), 4562 (2000).

34. F. Fuchs, U. Weimer, W. Pletschen, J. Schmitz, E. Ahlswere, M. Walter, J. Wagner, and P. Koidl, "High-performance InAs/$Ga_{1-x}In_xSb$ superlattice infrared photodiodes," *Appl. Phys. Lett.* **71**(22), 3251 (1997).

35. P.-Y. Delaunay, B. M. Nguyen, D. Hoffman, E. K.-W. Huang, M. Razeghi, "Background Limited Performance of Long Wavelength Infrared Focal Plane Arrays Fabricated From M-Structure InAs-GaSb Superlattices," *IEEE J. Quant. Electron.* **45**(102), 157-162 (2009).

36. H. S. Kim, E. Plis, J. B. Rodriguez, G. D. Bishop, Y. D. Sharma, L. R. Dawson, S. Krishna, J. Bundas, R. Cook, D. Burrows, R. Dennis, K. Patnaude, A. Reisinger, and M. Sundaram, "Mid-IR focal plane array based on type-II InAs/GaSb strain layer superlattice detector with nBn design," *Appl. Phys. Lett*. **92**(18), 183502 (2008).

37. C. L. Canedy, E. H. Aifer, I. Vurgaftman, J. G.Tischler, J. R. Meyer, J. H.Warner, E. M. Jackson, "Antimonide type-II "W" photodiodes with long-wave infrared R_0A comparable to HgCdTe, *J. Electronic Materials* **36**(8), 852-856 (2007).

38. M. Walther, R. Rehm, J. Fleissner, J. Schmitz, J. Ziegler, W. Cabanski, and R. Breiter, "InAs/GaSb type-II short-period superlattices for advanced single and dual-color focal plane arrays," *Proc. SPIE* **6542**, 654206 (2007).

39. C. J. Hill, A. Soibel, S. A. Keo, J. M. Mumolo, S. D. Gunapala, D. R. Rhiger, R. E. Kvaas, and S. F. Harris," Infrared imaging arrays based on superlattice photodiodes, " *Proc. SPIE* **6940**, 69400C (2008).

40. H. J. Haugan,F. Szmulowicz, G. J. Brown, and K. Mahalingam, "Band gap tuning of InAs/GaSb type-II superlattices for mid-infrared detection," *J. Appl. Phys.* **96**(5), 2580-2585 (2004).

41. H. Mohseni, E. Michel, M. Razeghi, W. Mitchel, and G. Brown, "Growth and characterization of InAs/GaSb type II superlattices for long-wavelength infrared detectors," *Proc. SPIE* **3287**, pp.30-37 (1998).

42. X. Cartoixà, D. Z.-Y. Ting, and T. C. McGill, "Description of bulk inversion asymmetry in the effective-bond-orbital model," *Phys. Rev. B* **68**(23), 235319 (2003)

43. David R. Rhiger, Robert E. Kvaas, and Sean F. Harris, and Cory J. Hill, "Characterization of LWIR Diodes on InAs/GaSb Type-II Superlattice Material," *Infrared Phys. Technol*. (2009), doi:10.1016/j.infrared.2009.05.009

44. J. Nguyen, D. Z.-Y. Ting, C. J. Hill, A. Soibel, and S. D. Gunapala, "Dark current analysis of InAs/GaSb superlattices at low temperatures," *Infrared Phys. Technol*. (2009). doi:10.1016/j.infrared.2009.05.022

45. B.-M. Nguyen, D. Hoffman, P.-Y. Delaunay, E. K.-W. Huang, M. Razeghi, and J. Pellegrino, *Appl. Phys. Lett*. **93**, 163502 (2008).

Downloaded from SPIE Digital Library on 29 Nov 2009 to 159.226.100.225. Terms of Use: http://spiedl.org/terms